Design and preliminary performance evaluation of a four wheeled vehicle with degraded adhesion conditions

Luca Pugi*

DIEF (Dipartimento Ingegneria Industriale),
Università degli Studi di Firenze,
Firenze, 50139, Italy
Email: luca.pugi@unifi.it
*Corresponding author

Francesco Grasso

DINFO (Dipartimento Ingegneria Informatica),
Università degli Studi di Firenze,
Firenze, 50139, Italy
Email: francesco.grasso@unifi.it

Marco Pratesi and Marco Cipriani

DIEF (Dipartimento Ingegneria Industriale),
Università degli Studi di Firenze,
Fi-renze, 50139, Italy
Email: marco.pratesi12@gmail.com
Email: marco.cipriani90@gmail.com

Argeo Bartolomei

Argos Engineering SRL,
Pistoia, 51100, Italy
Email: abartolomei@argosengineering.it

Abstract: Green shuttle vehicle (GSV) is a multi-purpose, four wheeled electric vehicle designed to operate in naturally protected areas where the conventional vehicles with internal combustion engines (ICEs) should be forbidden as a possible source of noise and pollution. The powertrain is based on a traction system with four in-wheel, permanent magnet motors that allow the vehicle to exhibit potentially interesting performances in terms of longitudinal dynamics, autonomy, and stability, even considering degraded adhesion conditions. In particular, this work also simulates the behaviour of the vehicle in degraded adhesion conditions, implementing a preliminary version of electric traction/braking fuzzy logic controller. The complete design and simulation of the system are an interesting example of how modern multi-disciplinary simulation tools can really accelerate the development of such a system with time and cost that are affordable also for small scale production series.

Copyright © 2017 Inderscience Enterprises Ltd.

Keywords: electric vehicle; direct drive technology; dynamical simulation; electric ABS system; modular traction system.

Reference to this paper should be made as follows: Pugi, L., Grasso, F., Pratesi, M., Cipriani, M. and Bartolomei, A. (2017) 'Design and preliminary performance evaluation of a four wheeled vehicle with degraded adhesion conditions', *Int. J. Electric and Hybrid Vehicles*, Vol. 9, No. 1, pp.1–32.

Biographical notes: Luca Pugi obtained his Master's degree in Mechanical Engineering in 1999 at University of Florence (Italy) and discussed his PhD thesis in 2003 at University of Bologna (Italy). Currently, he is a Researcher at the Mechatronic Lab of the University of Florence where he performs research and teaching activities for the courses of mechatronics and electric traction systems. His main research interests are currently devoted to mechatronics and vehicle dynamics. He is the author of about 200 of publications including journals, patents, and other kind of scientific products.

Francesco Grasso received his MSEE and a PhD in Electronic Devices and Circuits from the University of Florence, Florence, Italy, in 2000 and 2003, respectively. He is currently an Assistant Professor with the Department of Information Engineering (DINFO) at University of Florence. He teaches in the courses of Power Electronics for Smart Grids in the Master degree in Electrical and Automation Engineering. His research interests are in the areas of power electronics, renewable energy, power quality, circuit theory and neural networks. He is member of IEEE and advisor of AEIT.

Marco Pratesi received the Bachelor degree in Electronic Engineering, in 2012 and the MSc in Electrical and Automation Engineering from the University of Florence, in 2014. His main fields of interest are automotive, hybrid and electric vehicles, and control systems.

Marco Cipriani obtained the Bachelor degree in Electronic Engineering, in 2012 and the MSc in Electrical and Automation Engineering at the University of Florence, in 2014. His main fields of interests are automotive, control systems and electric project. Currently, he works in automation field for textile machinery.

Argeo Bartolomei deals with mechanical design in different sectors for 30 years. He is CEO of Argos Engineering SRL innovative SME that deals with research projects in various sectors including the electrical automotive. He holds several patents on Innovative Electric Vehicles like VIP (Innovative Multipurpose Vehicle) and other electric transport systems Mono-Rail like ButterFly (Innovative Automatic Guided Shuttle). Currently, he is committed in design, innovation and research on engine-wheels for traction of light and heavy ecological vehicles.

This paper is a revised and expanded version of a paper entitled 'Citation information the dynamics of vehicles on roads and tracks', *Proceedings of the 24th Symposium of the International Association for Vehicle System Dynamics (IAVSD 2015)*, Graz, Austria, 17–21 August, 2015.

1 Introduction: the green shuttle vehicle project

Environmental pollution and energy issues have caused a great deal of interest in electric vehicle (EV) solutions, especially in urban and ecological area transport. Conventional internal combustion engine (ICE) vehicles are a major source of urban pollution. Therefore, in the last years, research and development departments have been concentrating on EV's design. Recent electric motors development allows great advantages to EVs against traditional vehicles, as stated by Hori (2004): small and powerful electric motors can be installed into each wheel, so torque on each wheel, for a four in-wheel drive EV, can be quickly generated and independently controlled. Finally, electric motors can be controlled more precisely and easily than ICE. Urban centre restricted areas and ecological areas transportation issues have inspired the study of an electric vehicle that could overcome these problems. Green shuttle vehicle (GSV) is a multi-role vehicle able to transport people and goods, with a maximum load capacity of about 1000 kg, with remarkable off-road capacities to be used in wild or protected areas. So characteristics of GSV have to include high performances, versatility in terms of operating conditions and it should be innovative for current standards.

The aim of the project is to design the powertrain to realise a vehicle able to guarantee performances, autonomy and comfort necessary for a transportation application. The powertrain is based on a traction with four in-wheel drive that allows to avoid every type of mechanical transmission, to maximise the system efficiency, in particular regenerative braking, to increase free space within the main body of the vehicle and to simplify vehicle control. This architecture is studied in literature and several analyses on the performance and on the power management have been conducted: in particular in this study the works of Wang et al. (2011a), Watts et al. (2010), and Jain and Williamson (2009) have been considered.

Some more considerations concerning contributions available in literature and innovative contributions of the project will be further discussed within the description of the system in the following sections. Installing a motor in a rim produces rigid constraints in terms of space, so that the motor and drive electronics must both be power dense and compact. Moreover the motor must also offer high efficiency, low cogging torque and be intrinsically fail safe as described by Ifedi (2012). Moreover, electric motors have to be interfaced with the source of energy of the vehicle, the traction battery. This is the most critical in terms of choice and management; therefore to achieve a satisfactory autonomy of the vehicle it is necessary to design as efficient as possible a powertrain as described in the work of Young (2013).

Any motor requires a large external inverter/ power electronics unit, thus taking up space in the vehicle and reducing one of the key benefits of in-wheel motors, the increase in usable volume inside the vehicle body. Drive systems should be placed near the motor or directly connected to it in order to reduce power losses and electro-magnetic disturbances. In this work the design and some preliminary simulations concerning an electric vehicle called GSV with a direct drive traction system are presented.

GSV has to be a commercial vehicle; therefore, it is based on real components available in commerce, selected by attention to performances and economic value. Thanks to the proposed four-wheel direct drive layout the vehicle is able to exhibit potentially interesting performances in terms of longitudinal dynamics (high acceleration

and decelerations), autonomy (high transmission efficiency and full regenerative braking) and stability, even considering much degraded adhesion conditions. In particular, in this work, all these aspects are investigated using AMESim™ models in which the multibody mechanical behaviour, dynamic response of the traction system and on-board control system are simulated at the same time. Direct drive technology allows the development of a more effective traction control systems (TCS) and anti-lock braking systems (ABS). The goal of a TCS is providing maximum effective torque at wheels in every road condition. An ABS has the aim to control the wheel slip at an optimum value that can provide maximum tractive force during heavy braking. Vehicle performances are directly influenced by road conditions, on a slippery road effective torque should be adjusted reasonably to avoid slip or locking of wheels. Therefore, these control systems are used to improve vehicle safety in difficult weather or traffic conditions as well as the stability during high-performance driving. To preserve stability and performances of the vehicle with degraded adhesion condition an electric braking traction controller is implemented. The regulator is designed using Matlab-Simulink™, starting from the fuzzy logic approach proposed in the works of Wang et al. (2013a) and Yin et al. (2013) Compared to the approach proposed in literature, the authors have adapted this logic to their vehicle and have introduced some original contribution both in the structure of the controller and in the filter used to estimate wheel slip and vehicle longitudinal speed which were derived from previous experience matured by Pugi et al. (2006) and Meli et al. (2014) in the railway sector.

Powertrain and control system performances are evaluated through a co-simulation using Amesim™, and Matlab Simulink™. Amesim™ is used to design and simulate dynamical behaviour of the vehicle including powertrain and power electronics. Matlab-Simulink™ is used for design and implementation of control and filtering algorithm. The paper is organised as follows: the main features of the vehicle are introduced in Section 2, Section 3 explains about description and main features of the powertrain. Using simplified models, principle of operation and layout of the proposed system are introduced in Section 4. In Section 5, the detailed structure of the fuzzy controller is explained. In Section 6, performances and robustness of the proposed approach are tested on complete multibody model using the Amesim Icar™ environment. Finally Section 7 concludes the final considerations on performed work.

2 Vehicle specifications

Mechanical and electrical design characteristics of GSV are related to its specifications which are the following ones:

- weight: 1050 kg (Tare)
- maximum number of passengers: 7
- maximum speed: 90 km/h
- maximum acceleration: 0–90 km/h in 14 s
- autonomy: 150–200 km

- traction configuration: four in-wheel drive
- external radius of the tyre: 0.29 m
- internal radius of the tyre: 0.19 m
- chassis dimensions: 3.9 m × 1.8 m × 2.1 m.

GSV features allow obtaining a multi-role vehicle which should be used in a wide range of different operating scenarios: urban centres, ecological areas, golf clubs, high slopes or street with low adherence. Autonomy specifications allow an autonomy corresponding to a full day of service, so the recharge of batteries should be performed at night.

Four in-wheel drives ensure high efficiency, avoiding transmission and power losses and low weight at the powertrain. The external appearance and some encumbrance quotes of the vehicle are showed in Figure 1.

The vehicle is designed with the smallest dimensions as possible to transport until seven persons also in very narrow or crowded roads.

Figure 1 Main encumbrances of the simulated GSV vehicle (see online version for colours)

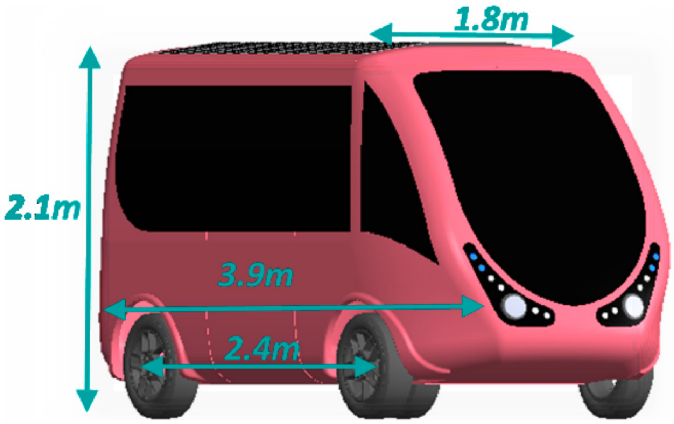

3 Powertrain design

Specifications of the vehicle introduced in Section 2 have to be translated in powertrain components to reach desired performances. The problem of the sizing of vehicle electric traction system has been widely studied: in particular in this work, sizing has been inspired by the previous contributions of Larminie and Lowry (2012), and Schaltz (2011).

First, it is necessary to size forces able to move the vehicle in all desired conditions; so a vehicle dynamics model should be introduced. This paper considers the model corresponding to equation (1) taken from Allotta and Pugi (2013)

$$F = m_t \ddot{x} + F_{\text{rot}} + F_d + mg \sin \alpha \tag{1}$$

where

F_{rot}: equivalent force corresponding to rolling resistances

F_i: aerodynamic lift force

F_d: aerodynamic drag force

F: total longitudinal traction force applied to the vehicle

m_t: vehicle mass considering inertia of rotating masses.

To calculate the torque requested to motors it is necessary to define a mission profile.

In this paper, the authors have adopted the European velocity profiles ECE UDC for urban cycles and NEDC for a mixed urban and extra urban cycle.

The following parameters concerning masses, losses and efficiencies are adopted in the preliminary design process:

- total mass: 2000 kg
- frontal area: 3.2 m^2
- air density: 1.3 kg/m^3
- rolling resistance: 0.01
- areodynamic penetration coefficient: 0.3
- traction efficiency: 0.85
- regenerative brake efficiency: 0.55.

Equation (1) allows to size the torque requested at the wheel to realise desired mission profiles, so in this way the nominal and maximum motor torque are calculated. Considering velocity profile and requested force it is possible to evaluate power at the wheels in order to evaluate an amount of power that should be stored in the traction battery. From this preliminary sizing it is possible to choose desired powertrain components. In this work both technical specifications and cost optimisation are evaluated to perform design and sizing of the system. A brief description of the electric power flow in the vehicle is visible in Figure 2. A list of components is represented in Figure 3. Finally, the corresponding scheme of the plant in terms of equivalent Amesim™ model (adopted for design and sizing) is represented in Figure 4. According to the scheme of Figure 2 the electric plant of the vehicle should be described in the following way:

- As a standard plug-in electric vehicle, GSV is charged using a external AC source (charge station), whose current is rectified and used to charge (AC/DC battery charger) the main power storage (batteries $LiFePO_4$) which feed a DC bus with a mean tension of 96 V.
- DC power from main batteries (DC Bus 96 V) is used to feed the inverters (4 × DC/AC) used to control the PMSM traction motors (4 × PMSM). Traction motors are also used to brake the vehicle during regenerative braking power can flow back from motors, through inverters and DC bus and finally to batteries.

- The same 96 V DC bus is also used to feed auxiliary systems such as air conditioning and to feed a step down chopper (DC/DC 96 →12 V) which provide the 12 V DC supply needed by most of the additional services of the car including most of the control logic systems (vital vehicle logic).

The low voltage circuit (DC Bus 12 V) is also connected to a backup battery (backup battery) and to a system of solar panels (solar panels) through a DC–DC converter (DC/DC charger MPPT). In this way most of the service of the vehicle including localisation and communication can work even if the main batteries are completely discharged or after a prolonged period of inactivity.

Figure 2 Main components and power flows of the electric plant

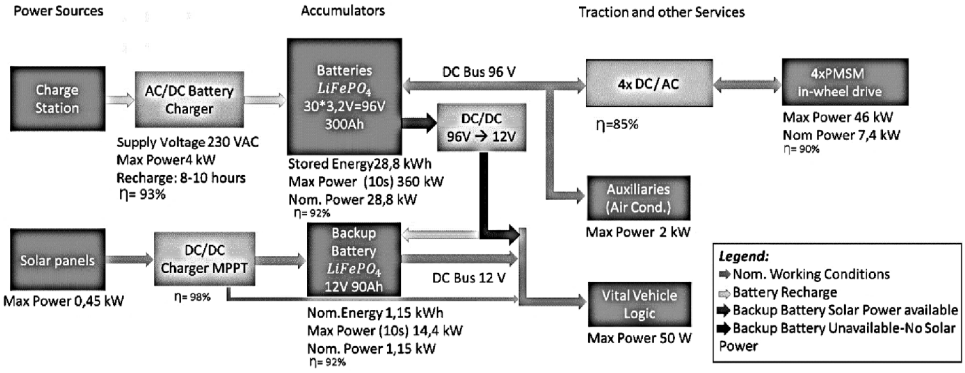

Figure 3 List of components adopted for the preliminary assembly of the GSV prototype (see online version for colours)

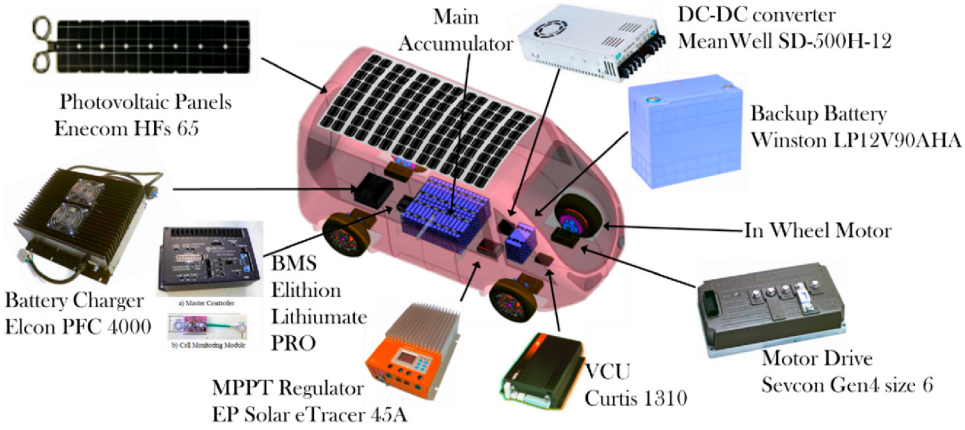

Considering both preliminary calculations and results from the complete simulation model of Figure 4, the expected range of the vehicle is at least 120 km on both ECE UDC and NUDC cycles even considering the consumption of air conditioning system and a very cautious management of energy storage system.

Figure 4 Corresponding Amesim model of the electric plant (see online version for colours)

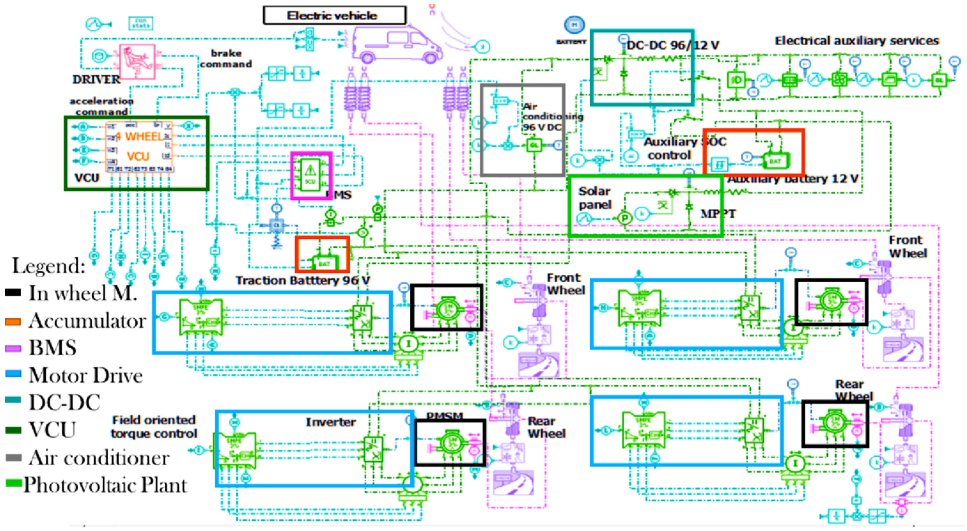

Some results of simulation and preliminary calculations are shown in Table 1.

Some additional results concerning mean efficiency of different components and adopted mission profile are visible respectively in Table 2 and Figure 5.

Table 1 Some preliminary calculations concerning autonomy of the vehicle

Mission profile	*Air conditioning*	*Autonomy* (km)	*Duration* (h)
ECE UDC Cycle	Full power	143	7.5
	No-air conditioning	205	11
NEDC Cycle	Full power	125	4
	No-air conditioning	160	5.5

Table 2 Corresponding mean efficiency of powertrain components evaluated for the ECE NEDC cycle visible in Figure 5

	Components	*Component efficiency* (%)	*Complessive efficiency* (%)
Traction	Battery	90	90
	Inverter	91	82
	PMSM	89	73
Reg. braking	PMSM	85	85
	Inverter	85	72
	Battery	80	58

Figure 5 ECE NEDC cycle vehicle speed and corresponding motor torque profiles (see online version for colours)

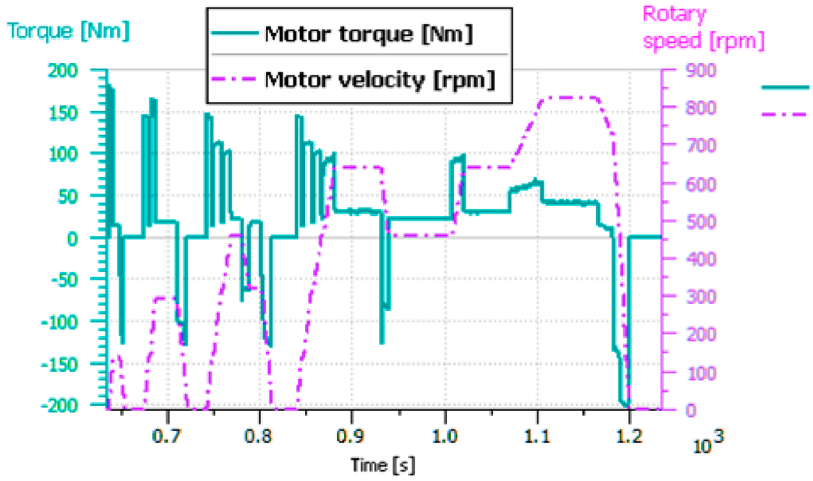

4 Preliminary considerations on vehicle dynamics and traction

This section presents the quarter vehicle model that it is quite useful to understand design and principles of operation of the proposed TCS and ABS controllers. Then the planar vehicle dynamics model that has been preliminary used to understand the dynamical behaviour of the during running is briefly described. Finally, above-described models are used to explain the way in which vehicle longitudinal speed and state for the wheel-road contact should be in some-way estimated online.

4.1 Degraded adhesion conditions and quarter vehicle model: some preliminary considerations

The way in which longitudinal dynamic of a vehicle should be affected by the modulation of torque exerted on wheels during a traction or braking manoeuvre with degraded adhesion conditions, should be easily explained using the so-called quarter vehicle model.

Quarter vehicle model considers the longitudinal behaviour of a single-wheeled vehicle shown in Figure 6. In this simplified model, drag force and rolling resistances are neglected, so the dynamical behaviour of the system is represented by the system of equations (2) which are also commonly adopted on handbook such as the one of Jazar (2008) but also in a wide range of applications which are inherent to the topics of this works such as the works on four-wheeled electric vehicles of Wang et al. (2011b) and Feiqiang et al. (2009):

$$\begin{aligned} m\ddot{x} &= F_x \\ J\dot{\omega} &= T_m - F_x r \\ F_x &= \mu(\lambda) mg, \end{aligned} \tag{2}$$

where m is the load mass on each wheel m (M is the total mass of the vehicle), $\dot{x}$ is vehicle speed, F_x is the traction force related to road friction μ, J is wheel inertia, $\dot{\omega}$ is angular acceleration, T_m is the torque applied to the wheel and r is the external radius of the tyre. Obviously in a real vehicle the value of m depends from the mass distribution of the vehicle and from the dynamical load transfers owing to inertial forces.

Figure 6 Quarter vehicle model

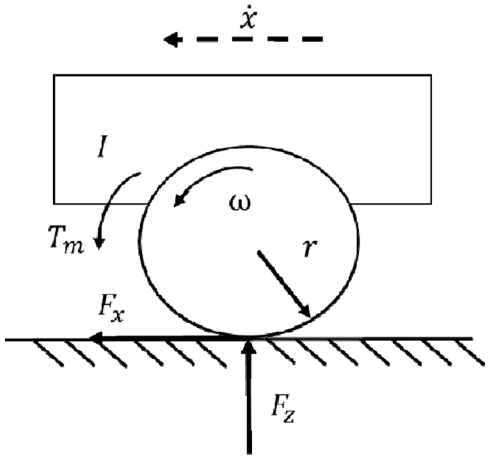

This model considers an adherence coefficient $\mu(\lambda)$ which depends from slip ratio λ which is usually defined in equation (3)

$$\begin{cases} \lambda = \dfrac{\omega r - \dot{x}}{\omega r}; & \text{Traction} \\ \lambda = \dfrac{\omega r - \dot{x}}{\dot{x}}; & \text{Braking} \end{cases} \tag{3}$$

Most of the commonly wheel-road adhesion models such as magic formula introduced from Pacejka and Bakker (1992) assume a behaviour of the friction factor as the one represented in Figure 7. The value of $\mu(\lambda)$ is maximum for a particular value of λ called λ_{opt}. As a consequence, the aim of an ASR in traction or an ABS during braking should be to keep slip coefficient within a range around λ_{opt}. By regulating the exerted torque on wheel T_m ASR/ABS regulator are then able to maximise vehicle performances in terms of longitudinal accelerations avoiding wheel-lock (braking manoeuvres) or more generally excessive sliding (both traction and braking manoeuvres). For a four in-wheel motor like GSV this kind of regulation can be easily performed both during traction and braking. It should also be noticed that in case of severe degradation of adhesion conditions, the shape of adhesion curves is quite flat and the identification of an optimal value λ_{opt} should produce quite erratic and unstable results. On the other hand, the identification of λ_{opt} is easier with good adhesion conditions where the knowledge of the exact value of λ_{opt} is less important for system performances. For this reason, identification algorithms aiming to identify online the λ_{opt} value that have been recently proposed in literature Ko et al. (2014) should be carefully evaluated and tested in terms of robustness especially considering highly degraded conditions or hybrid scenario with the fast transients between slippery and good contact conditions.

Figure 7 Relationship between adherence and slip coefficients

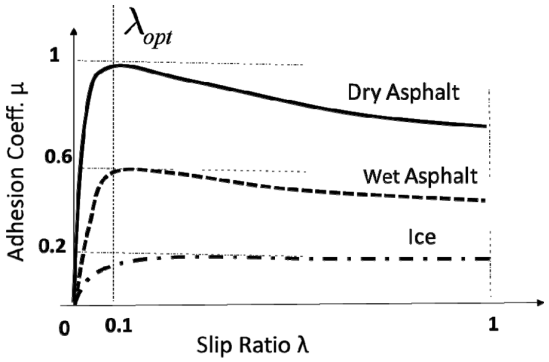

4.2 Planar vehicle model: some preliminary considerations for the design of the system

Degraded adhesion conditions should also negatively affect the stability of the vehicle producing potentially dangerous effects. To consider vehicle dynamics involved in the control problem analysed, it should be considered three degree-of-freedom model visible in Figure 8: only longitudinal and lateral motions and yaw rotation are considered (vertical, pitch and roll motions are ignored). This is the most commonly adopted model for the study of vehicle directional stability such as the work of Wang et al. (2011a, 2011b) or Jazar (2008).

Figure 8 Planar vehicle model (3D.O.F.)

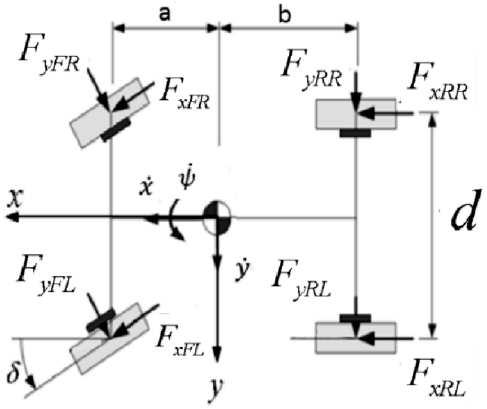

The model of Figure 8 neglects the difference between the steering angles of left and right wheels (δ_L, δ_R) considering a mean steering angle δ defined in equation (4):

$$\cot\delta = \frac{\cot\delta_L + \cot\delta_R}{2}; \tag{4}$$

Equations that describe vehicle behaviour considered in this paper are expressed in equation (5).

$$\begin{aligned}
m(\ddot{x}-\ddot{y}\dot{\psi}) &= (F_{xFL}+F_{xRR})\cos\delta-(F_{yFL}+F_{yFR})\sin\delta+(F_{xRL}+F_{xRR})\\
m(\ddot{y}-\ddot{x}\dot{\psi}) &= (F_{yFL}+F_{yFR})\cos\delta-(F_{xFL}+F_{xFR})\sin\delta+(F_{yRL}+F_{yRR})\\
I_x\ddot{\psi} &= \left[(-F_{xFL}+F_{xFR})\cos\delta+(F_{yFL}-F_{yFR})\sin\delta+(-F_{xRL}+F_{xRR})\right]\frac{d}{2}\\
&\quad -(F_{yRL}+F_{yRR})b+\left[(F_{yFL}+F_{yFR})\cos\delta-(F_{xFL}+F_{xFR})\sin\delta\right]a,
\end{aligned} \tag{5}$$

where subscripts x, y are used to indicate respectively longitudinal and lateral directions, FL, FR, RL and RR represent front and rear tyres; $\dot{\psi}$ indicates yaw rate, δ is the vehicle steering angle; d represents the track of the vehicle and a, b represent respectively distances of the centre of gravity from front and rear axle.

As visible by equation (2) longitudinal acceleration of the vehicle is heavily affected by longitudinal forces (F_{xFL}, F_{xFR}, F_{xRL}, F_{xRR}) exchanged between wheels and road. On the other hand, the yaw rotation dynamics is highly affected by both lateral and longitudinal forces. In particular a regulator able to regulate exerted torques on wheels and consequently longitudinal forces on tyres should be to correct the yaw rotation producing a correction action M_ψ which can be approximately evaluated using equation (6), which is can be easily obtained from equation (5):

$$M_\psi = \left[(-F_{xFL}+F_{xFR})\cos\delta+(-F_{xRL}+F_{xRR})\right]\frac{d}{2}-\left[(F_{xFL}+F_{xFR})\sin\delta\right]a. \tag{6}$$

By differentiating the torque applied on left wheels with respect to right ones it is possible to correct the yaw of the vehicle. This is not the only way in which a regulator should improve vehicle stability since an optimal regulation of wheel sliding should naturally produce improvements in terms of vehicle stability. This effect should be easily explained by adopting the simplified friction ellipse model as described by Jazar's (2008) handbook. The model is described in equation (7).

$$\left(\frac{F_{xij}}{F_{xij\max}}\right)^2+\left(\frac{F_{yij}}{F_{yij\max}}\right)^2=1. \tag{7}$$

In equation (7), F_{xij} and F_{xij} represent longitudinal and lateral forces of the tyres identified by the corresponding i and j indices, and $F_{xij\max}$ and $F_{xij\max}$ are the corresponding maximum values that can be transmitted in longitudinal and lateral directions according limitation on available friction factor μ and vertical F_{zij} as defined in equation (8).

$$\begin{aligned}
F_{xij\max} &= \mu_x F_{zij};\\
F_{yij\max} &= \mu_y F_{zij}.
\end{aligned} \tag{8}$$

Looking at equation (8) it should be noticed that the maximum tangential forces that can be exerted on tyres are also influenced by vertical load transfers between wheels. However, considering a severe degradation of adhesion conditions, also corresponding vehicle accelerations and consequently load transfers between wheels should be considered quite limited. Lateral stability of the vehicle should be also improved by the fact that the controller in order to avoid high-longitudinal sliding should reduce the applied longitudinal forces to a value F_{xij} which is lower than the maximum one ($F_{xij\max}$). As a consequence, looking at the typical shape of the friction ellipse, for an

assigned value of F_{xij} it should be possible to apply also a lateral force, whose maximum possible value $F_{yij\max*}$ represented in Figure 9 should be not so negligible and should contribute to enhance the lateral stability of the vehicle. In this way, it is possible to understand how even a simple system devoted only to control longitudinal dynamics should also contribute to improve the directional stability of the vehicle. The simplified model of friction ellipse is often used also in very recent publications such as Ko et al. (2014), since it is a good way to understand the combined effect of combined lateral and longitudinal efforts on wheel road contact interface.

Figure 9 Friction ellipse (see online version for colours)

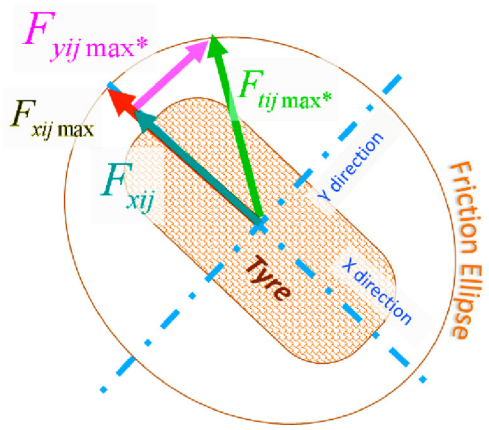

4.3 Vehicle speed and wheel state estimation

Available adhesion on wheels cannot be directly measured but only roughly estimated from indirect measurements of wheel and vehicle dynamics. There are some references concerning, for example, sliding mode observers to reconstruct wheel road contact forces, such as in the work of M'Sirdi et al. (2007), or adaptive technique for the online identification of adhesion conditions as stated in the work of Geamanu et al. (2011).

Also the direct measurements of vehicle speed should be quite unreliable when degraded adhesion conditions occur. In particular, according to equation (9), with good adhesion conditions the sliding of each wheel λ_{ij} should be small so also lateral and longitudinal sliding λ_{xij} and λ_{yij} should be quite small. Two main consequences should be derived:

- the longitudinal speed of the vehicle is proportional to the rotational speed of wheels
- lateral sliding is quite small and the kinematic relationship between steer angle and corresponding yaw/directional behaviour of the vehicle is approximately verified.

$$\lambda_{ij} \approx 0 \begin{cases} \lambda_{xij} \approx 0 \Rightarrow \dot{x} \approx \omega_{ij} r \\ \lambda_{yij} \approx 0 \Rightarrow \begin{cases} \dot{y} \approx 0 \\ \beta = a\tan\dfrac{\dot{y}}{\dot{x}} \approx 0 \end{cases} \end{cases} \tag{9}$$

When degraded adhesion occurs relation (9) is not verified, for this reason the authors adopted for the estimation of the longitudinal speed of the vehicle the estimation scheme of Figure 10.

Figure 10 Vehicle speed estimation (see online version for colours)

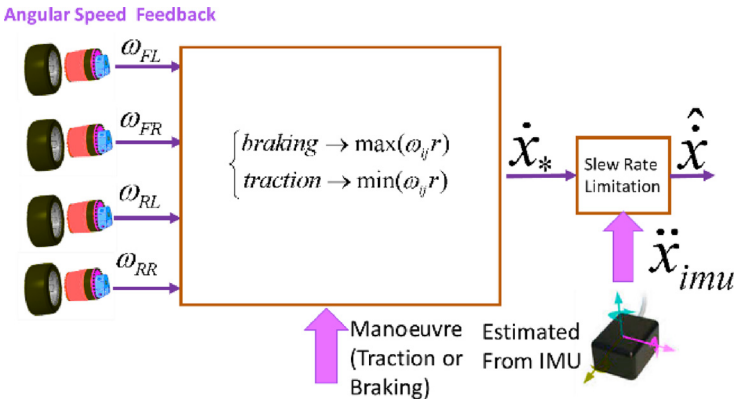

Angular speed of each wheel is measured, using the angular feedback of each motor drive. According to the definition of longitudinal sliding equation (3), positive sliding is expected with a traction manoeuvre and negative one during braking. As a consequence, according to the current manoeuvre state (traction or braking), the wheel with maximum (traction) or the minimum (braking) rotational speed should correspond to the one with the minimum value of $|\lambda_{xij}|$. The peripheral speed of the wheel ($\omega_{ij} r$) with the lowest value of $|\lambda_{xij}|$ is the best approximation of the vehicle longitudinal speed $\dot{x}_*$. However, in the case of very degraded adhesion conditions the estimation $\dot{x}_*$ should be affected by heavy errors since the minimum value of $|\lambda_{xij}|$ should not be negligible. To further improve the estimation of the longitudinal speed, the measurement of the longitudinal acceleration $\ddot{x}_{imu}$ is used to perform a slew-rate limitation of the estimated speed profile according to equation (10).

$$\begin{aligned} &\text{if } |\ddot{x}_*| > |\ddot{x}_{imu}| + tol \Rightarrow \hat{\dot{x}}(t + \mathrm{d}t) = \dot{x}_*(t) + \ddot{x}_{imu}(t)\,\mathrm{d}t \\ &\text{else } \hat{\dot{x}}(t) = \dot{x}_*(t) \end{aligned} \tag{10}$$

According to equation (10), if the estimated deceleration/acceleration $|\ddot{x}_*|$ is too high with respect to the measured longitudinal acceleration then the estimated speed $\hat{\dot{x}}$ is calculated by integrating the measured longitudinal acceleration $\ddot{x}_{imu}$. The *tol* threshold is introduced to improve the robustness of the system with respect to bias errors of sensors. In this work, the longitudinal acceleration $\ddot{x}_{imu}$ is supposed to be estimated acceleration provided by a commercial inertial measurement unit (IMU). The IMU solution has been chosen considering the commercial availability of pre-calibrated systems in which most of the work concerning filtering and estimation algorithms needed to obtain reliable orientation and acceleration measurements (advanced filtering of tri-axial accelerometers and gyros optional data fusion with GPS and magnetometer) is directly provided by the developer of the commercial platform. A good reference concerning the methods that should be adopted to perform a good estimation of the longitudinal acceleration rejecting

effect owing to other spurious disturbances like slope of the road or car body pitch should be found in the work of Tanelli et al. (2006).

Once the estimation $\hat{\dot{x}}$ of the longitudinal speed is known it is also possible to calculate the estimated longitudinal sliding of the wheels defined according to equation (11):

$$\begin{cases} \hat{\lambda}_{xij} = \dfrac{\omega_{ij} r - \hat{\dot{x}}}{\omega_{ij} r}; & \text{Traction} \\ \hat{\lambda}_{xij} = \dfrac{\omega_{ij} r - \hat{\dot{x}}}{\hat{\dot{x}}}; & \text{Braking} \end{cases} . \tag{11}$$

Knowing the estimated value of longitudinal sliding of each wheel it is then possible to understand the current state of the wheel with respect to a known feasible/recommended range of values.

5 Design of the fuzzy control system

For the design of the control systems, the authors supposed the availability of the following feedback/measurements and actuations corresponding to the simplified layout of Figure 11:

- Angular speed measurements of wheels provided by motor drives.
- Estimation of vehicle car body accelerations and rotations provided, as previously introduced, by a smart commercial IMU.
- Complete feedback concerning the manoeuvre performed by the driver (traction or braking state, steer angle, etc.).
- Both traction and braking efforts are totally exerted by electric actuators to minimise wear of braking pad material and to maximise vehicle autonomy with a full regenerative braking. Mechanical brakes are installed but their use is limited to parking in nominal conditions. In case of partial failure of motor drive system mechanical brakes should be used as backup unit for a vehicle whose traction performances are reduced by about 50% with respect to their nominal levels.

In most recent works available in literature such as the one of Ko et al. (2014), traction/braking controllers are modelled as complex multiple input, multiple output (MIMO) controllers in which complex online estimators are used to evaluate wheel road contact forces, available adhesion, and other important parameters that are used by model-based controllers to optimise the torque correction pattern ordered to the in-wheel motor drives.

In this work the authors preferred to avoid complex model-based estimations and complex controllers with heavy cross-coupling effects between different parts of the regulator considering mainly for two reasons:

- Limited production series and high level of customisation of the proposed applications: limited production series do not justify prolonged experimental campaigns. Heavy customisation level produced involves a high variability of the features of the produced vehicle, further increasing the need of simpler and robust solutions.

- Robustness and stability of this kind of algorithms with respect to high variability scenarios have to be really demonstrated: as is quite common in real operating condition the rapid transition between parts of the road with different adhesion conditions (as example a slippery iced part over a road which have mean or good adhesion conditions) in which the advantage of complex filtering algorithms is to identify the current mission conditions is almost nullified. Also control algorithms that heavily depend on a good identification of the controlled system should be heavily affected in terms of robustness by parametric uncertainties (first of all uncertainties concerning model, wear and inflation pressure of tyres or the real state of the road surface).

Figure 11 Simplified layout of the proposed traction/braking controller (see online version for colours)

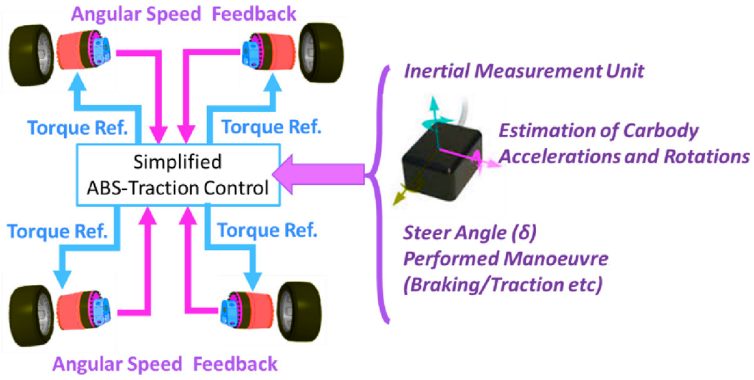

For these reasons, the controller is organised in three main sub-components visible in Figure 12 that can be easily tuned independently acting on a limited set of parameters:

- *Vehicle speed/state estimation*: this block previously described in Section 4.3 is able to estimate vehicle speed, and longitudinal sliding of wheels.
- *Wheel sliding correction*: according to the estimated sliding of each wheel the controller tries to modulate applied torque to keep the absolute value of wheel road sliding around an optimal value λ_{opt} of about 0.15. This value is often used in literature in the recent works of Wang et al. (2011c, 2013b) and it is quite realistic also considering the shape of adhesion curves visible in Figure 7. The action of the regulator is performed by modifying the reference torque pattern T_{ref} imposed by the human driver with the correction vector ΔT_{ASR}. In this way, the corrected torque output T_{ref*} is a vector composed by four scalar components $T_{ref\ *ij}$ each corresponding to the corrected torque reference of the *ij* wheel.
- *Yaw angle correction*: with an approximated estimation of current vehicle speed and steer angle, it is possible to calculate a range of admissible values of the yaw rate $\dot{\psi}$. If the estimated value $\hat{\dot{\psi}}$ exceeds this range the controller should correct the torque reference applied to left and right wheels to stabilise vehicle trajectory. Also in this case a correction vector ΔT_{YAW} is produced by the regulator and used to produce a corrected torque reference vector T_{ref**}

Figure 12 Main components of the proposed regulator (see online version for colours)

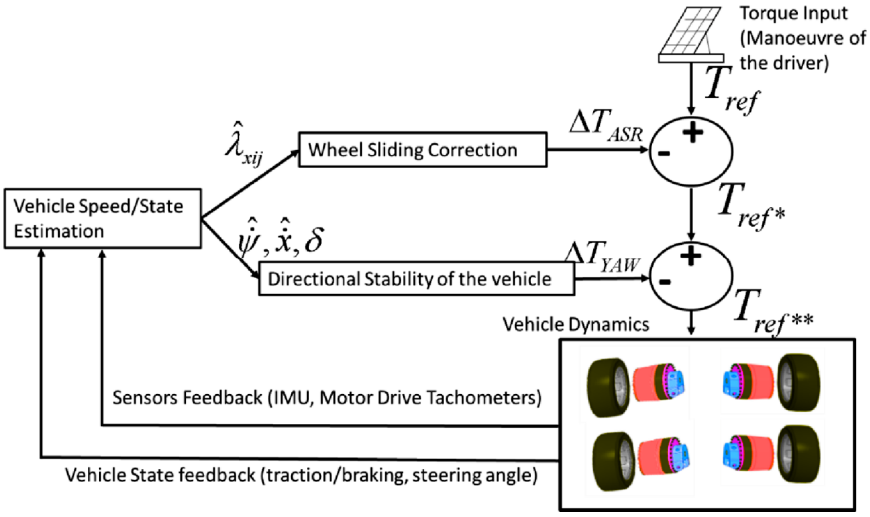

5.1 Fuzzy implementation of the wheel sliding correction block

Both the control stages visible in Figure 12 are implemented in terms of fuzzy logic. Authors chose this kind of implementation since fuzzy logic should be the ideal choice for the control of process poorly structured or modelled and heavily affected by uncertainties both in terms of modelling or decision management.

This definition is clearly applicable to tyre road interaction especially with degraded adhesion conditions where the adoption of simple and robust controllers is quite mandatory.

Also in literature, the authors find many recent studies in which fuzzy logic is adopted for the design of TCS of four in-wheel drive vehicles such as in the works of Yin et al. (2013) and Feiqiang et al. (2009).

In particular the solution proposed by for the development of a yaw controller (visible in the scheme of Figure 12) as proposed Feiqiang et al. (2009) has being considered in this work while the one proposed by Yin et al. (2013) inspired the design of the wheel sliding correction (visible in the scheme of Figure 12).

In the above cited works authors integrated both the regulation algorithms in a single application, introduced significant improvement to increase system robustness and validated their results using a full vehicle model developed using Amesim Icar™ whose parameters where mostly unknown for the internal logic of the proposed controller.

In particular wheel sliding correction block was developed using Matlab Simulink 'FuzzyLogicDesigner™', the structure of the regulator is visible in Figure 13:

- By comparing the desired longitudinal sliding λ_{opt} with the corresponding estimated value for the *ij* wheel it is possible to evaluate the corresponding error $e(\lambda_{xij})$ and its filtered derivative.
- Two antecedent membership functions with the associated fuzzy sets visible in Figure 13 are defined with respect sliding error $e(\lambda_{xij})$ and its first derivative.

- Once the corresponding state is calculated through the inference rules/table represented in Figure 13 the correction ratio ΔT_{rel_ij} of the reference applied to the *ij* wheel is extracted according the consequent membership function also visible in Figure 13. The admissible values of ΔT_{rel_ij} are restricted to the interval [–1, 1] since the corresponding correction ΔT_{ASRij} has to be limited in the range $[-T_{ref}, T_{ref}]$.

The surface corresponding to the behaviour of relative correction ΔT_{rel_ij} with respect to the tabulated values of errors and error derivative are visible in Figure 14: the resulting controller is very similar to a gain scheduled proportional derivative controller of estimated longitudinal slip of the wheel.

It should also be noticed that the action of the controller is scaled with respect to desired torque reference of the human driver; in this way when a skilled human driver recognises a degraded adhesion condition and perform a reduction of the traction/braking demand, also the controller scale takes corrective action improving the overall stability of the control loop.

Figure 13 Detail of the wheel sliding correction fuzzy controller (see online version for colours)

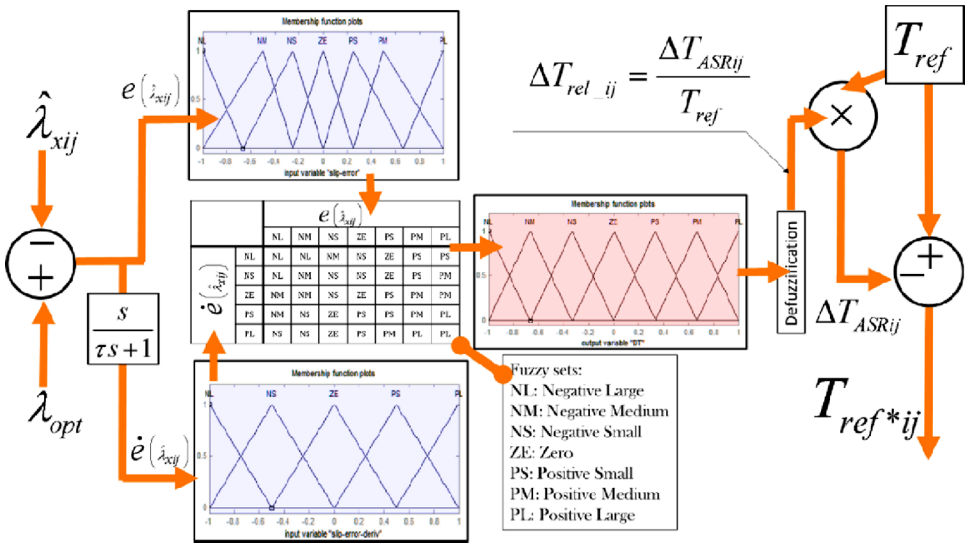

Figure 14 Tabulated surface of relative correction respect to the error and error derivatives of wheel slip (see online version for colours)

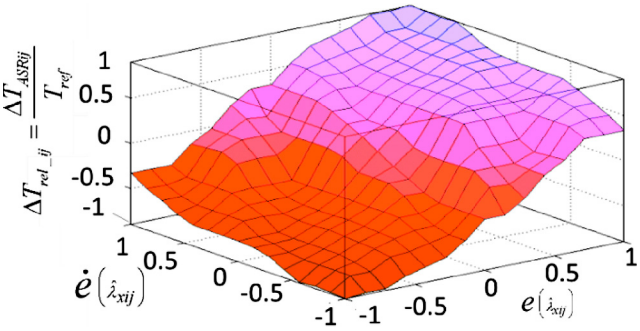

5.2 Fuzzy implementation of the yaw/directional stability controller

Referring to the simplified model of Figure 8, to evaluate the stability of the vehicle both the yaw rate $\dot{\psi}$ and the lateral speed $\dot{y}$ are often expressed in terms of relative lateral slip ratio β defined according to equation (12)

$$\beta = \frac{\dot{y}}{\dot{x}}. \tag{12}$$

The estimation of $\dot{\psi}$ is quite easy: measurements are performed with gyros also considering that low frequency components corresponding to near to static values are not of practical interest for the control of the vehicle stability so components corresponding to gyros offsets should be easily rejected.

On the other hand, the measurement of the lateral speed $\dot{y}$ from integration of inertial measurement should be more affected by larger estimation errors.

For this reason, authors have developed the control scheme visible in which it is currently implemented a partial scheme which take count only of yaw rate.

In particular authors adopt an estimated optimal value of $\dot{\psi}$, called $\hat{\dot{\psi}}_{\text{opt}}$ defined according to equation (13)

$$\hat{\dot{\psi}}_{\text{opt}} = \frac{\hat{\dot{x}}}{(a+b)\left(1+\dfrac{\hat{\dot{x}}}{v_{ch}}\right)} \tan\delta. \tag{13}$$

Equation (13) is written considering the kinematic model of Figure 8, the v_{ch} term should be customised to roughly approximate drift effects ($v_{ch} = \infty \Rightarrow$ ideal steering).

According to the scheme of Figure 15 the optimal reference yaw rate and the measured one are used to generate an error signal which is processed using a fuzzy controller designed with the same tools and methods previously described for the wheel sliding correction block: a pre-processing through an antecedent membership function, a table of inference rules, consequent membership functions and de-fuzzification process to produce the corresponding action of the regulator. In this second stage, the regulator produces an action ΔT_{rel_ψ} defined according in equation (14).

$$\Delta T_{rel\_\psi} = \frac{\Delta T_{YAWiR}}{T_{ref*iR}} = -\frac{\Delta T_{YAWiL}}{T_{ref*iL}} \tag{14}$$

As a consequence the corresponding corrections ΔT_{YAWij} and the final torque references for in wheel motors $T_{ref**ij}$ on each wheel are defined in equation (15)

$$\begin{aligned}
&\Delta T_{YAWFR} = \Delta T_{rel_\psi} T_{ref*FR} \Rightarrow T_{ref**FR} = T_{ref*FR} - \Delta T_{YAWFR} \\
&\Delta T_{YAWRR} = \Delta T_{rel_\psi} T_{ref*RR} \Rightarrow T_{ref**RR} = T_{ref*RR} - \Delta T_{YAWRR} \\
&\Delta T_{YAWFL} = -\Delta T_{rel_\psi} T_{ref*FL} \Rightarrow T_{ref**FL} = T_{ref*FL} - \Delta T_{YAWFL} \\
&\Delta T_{YAWRL} = -\Delta T_{rel_\psi} T_{ref*RL} \Rightarrow T_{ref**RL} = T_{ref*RL} - \Delta T_{YAWRL}
\end{aligned} \tag{15}$$

Also in this case the fuzzy regulator should be approximated as a gain scheduled regulator of vehicle yaw rate, with a correction that is proportional to the current torque reference after the correction performed by the ‘sliding correction block’. In this way,

in case of degraded adhesion conditions, the performed corrections should be higher on wheels with bigger torque references corresponding to better adhesion conditions. This is a highly desirable behaviour in terms of robustness and stability of the proposed control system.

Figure 15 Scheme of the implemented YAW directional stability controller (see online version for colours)

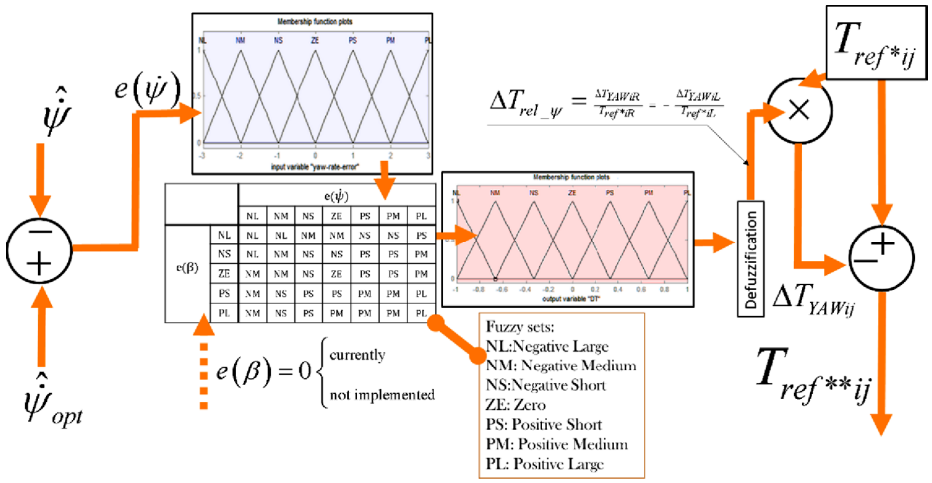

6 Simulation results

To verify the performances and the robustness of the proposed controller, authors implemented a full three-dimensional model of the vehicle using Amesim™ and in particular the ICAR module visible in Figure 16. The model is composed by the following sub-components:

- *Multi-body model of the vehicle*: 15 degrees-of-freedom are modelled. In particular, the chassis/car body is modelled as a six degree-of-freedom rigid body, additional eight degree-of-freedom are added to model both rotations of wheels and deformation of suspensions, the last degree of freedom is introduced to model the steering of forward wheels. Main parameters of the multibody models are visible in Table 3.
- *In wheel motors*: four quadrant performances of the traction motors are modelled.
- *Tyre-road interaction*: the full three-dimensional interaction between wheel and road is simulated adopting the Pacejka and Bakker (1992) magic formula approach, adhesion levels are tabulated as function of the position of the vehicle along the road to simulate different adhesion patterns.
- *Fuzzy controller*: Fuzzy controller logic described in previous sections is implemented in Mathworks Simulink™ and contextually executed with the Amesim vehicle model in co-simulation mode: at a fixed communication frequency of 1 kHz, the model of the vehicle controller takes simulated measurements from Amesim sensor blocks, decides the correction of torque reference according to the previously

described logic and provide torque reference commands to simulated motors. Data transfer and contextual execution of the Amesim model of the vehicle with the fixed step regulator implemented in Matlab Simulink is automatically handled by the so-called "Amesim Co-Simulation Interface". In this way it is also possible to take count in the simulation of delays and limited bandwidth effects introduced by the discrete-fixed step implementation of control logic. It is also interesting to notice that principle of operation of the proposed controller have been designed both simplified road tyre adhesion and vehicle models described in previous sections that are much simpler respect to the complete Amesim model adopted to perform the simulation and to obtain the results described in this section. As consequence the proposed simulation tests should be considered as quite significant in terms of robustness of the proposed approach respect to parametric uncertainties.

Figure 16 Main components of Amesim model of the vehicle with Simulink co-simulation of the fuzzy controller (see online version for colours)

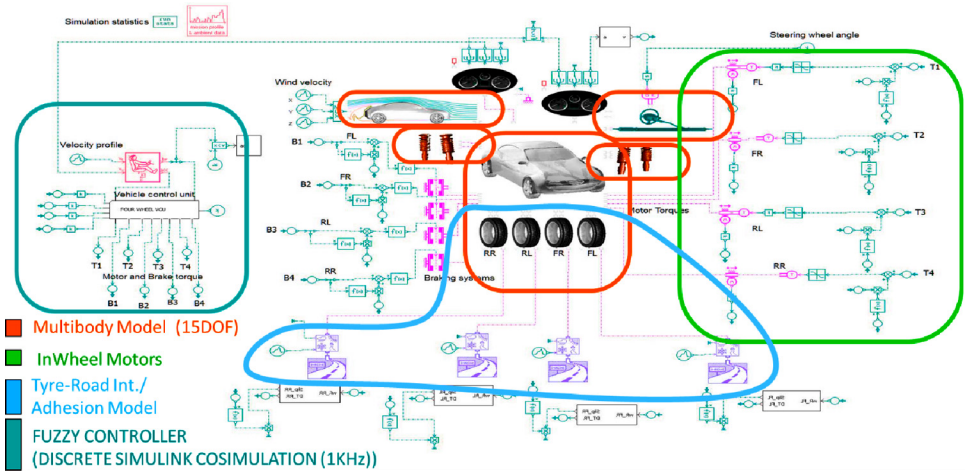

Table 3 Main properties of the vehicle multibody model

Property	*Value*	*Property value*	
Suspended mass (carbody)	1800 [kg]	Base $l = a + b$	2400 [mm]
Unsuspended masses (wheels)	60 [kg] (each wheel)	t (track)	1450 [mm]
I_{xx} Inertia of carbody	600 [kg m^2]	Pos of centre of mass (x_g, y_g, z_g)	1200, 0, 450 [mm]
I_{yy} Inertia of carbody	2400 [kg m^2]	Suspension stiffness	26,000 [N/m]
I_{zz} Inertia of carbody	2300 [kg m^2]	Suspension damping	26,000 [Ns/m]
Wheel rolling radius	290 [mm]		

Performance of the proposed controller has been tested both for braking and traction manoeuvres.

For simulated traction manoeuvres tests are performed considering accelerations from standstill to various targets of velocity until the maximum of 90 km/h. Simulations are

repeated in different road conditions, such as $\mu = 0.8$ corresponding to dry road, $\mu = 0.5$ for wet road and $\mu = 0.2$ corresponding to snowy road. Results obtained with different adhesion levels are compared in terms of travelled distance needed to reach an assigned speed. Same adhesion conditions are also adopted for the simulation of braking tests from different initial speed to vehicle stopping conditions. For braking tests, results are compared in terms of stopping distance.

Results of performed tests are summarised in Table 4: each test is repeated simulating also the case in which the proposed control system is not installed and the torque reference ordered by the human driver is directly transmitted to motors without any further correction.

Table 4 Comparison of some simulation tests considering different road conditions, system configurations and performed manoeuvres

		Vehicle without control (*distance to reach target speed*)			*Vehicle with ASR control* (*distance to reach target speed*)			
		μ = 0.8	*μ = 0.5*	*μ = 0.2*	*μ = 0.8*	*μ = 0.5*	*μ = 0.2*	
Final speed (acceleration)	90 km/h	143.3 m	143.3 m	Unstable	143.3 m	143.3 m	231.3 m	
	70 km/h	92.6 m	92.6 m	Unstable	92.6 m	92.6 m	146.8 m	
	50 km/h	45.0 m	45.0 m	Unstable	45.0 m	45.0 m	67.2 m	
	30 km/h	17.7 m	17.7 m	Unstable	17.7 m	17.7 m	24.6 m	
								$\frac{x_{\text{stop}}}{x_{\text{ideal}}}(\mu = 0.2)$
Launch speed (braking)	90 km/h	127.4 m	127.4 m	Unstable	127.4m	127.4 m	189.9 m	1.19
	70 km/h	82.5 m	82.5 m	Unstable	82.5 m	82.5 m	119.0 m	1.23
	50 km/h	40.6 m	40.6 m	Unstable	40.6 m	40.6 m	61.0 m	1.24
	30 km/h	15.0 m	15.0 m	Unstable	15.1 m	15.1 m	22.4 m	1.26

It is interesting to notice that for adhesion levels corresponding to a wheel road friction factor μ greater than 0.5 vehicle performances are clearly not affected by a light reduction of the friction factor.

In case of very degraded adhesion conditions, the simulation of vehicles without the proposed control system produce directional instability of the vehicle with potential catastrophic effects in terms of safety. On the other hand, simulations of vehicles equipped with the proposed controller show a slight increase in term of stopping distance and a great directional stability. The system both in degraded and nominal adhesion is designed to have higher braking performances with respect to traction ones. From a safety point of view, one of the most interesting features is the increase of braking distance x_{stop} with respect to an ideal nominal value x_{ideal} that can be calculated according to equation (16) considering a known adhesion coefficient μ, the starting speed $\dot{x}_{init}$. In equation (16) an optimal distribution (between wheels) and application (no delays) of braking efforts are also supposed.

$$x_{\text{ideal}} = \frac{1}{2}\frac{\dot{x}_{\text{init}}^2}{\mu g}. \tag{16}$$

As visible in Table 4, the ratio between x_{stop} and x_{ideal} is not too penalising.

Concerning directional stability, in Figure 17, the braking trajectories of the vehicle with and without the proposed control system are compared: the two trajectories are referred to a braking manoeuvre from an initial velocity of 90 km/h with a simulated friction coefficient of 0.2. It is interesting to notice that the regulator is able to reduce the lateral displacement of the vehicle to few centimetres with respect to a total braking distance of about 190m. In particular on the left side of Figure 17, it is also shown a detail of the rendering of the unstable vehicle at the end of braking phase including the graphical representation of the forces exchanged between road and wheels. Corresponding wheel speed and applied torque profiles (frontal right wheel) are shown in Figures 18 and 19. It should be noticed the relative smooth behaviour of the exerted torque profiles which should make relative easier also the blending with conventional hydraulic or pneumatic brakes. Simulated trajectories of the vehicle considering full traction from 0 km/h to 90 km/h with different configuration of the controller are also visible in Figures 20 and 21: in particular, in order to make more evident the effects of different terms of the proposed controller, the simulated trajectory of the proposed regulator is also compared with the results corresponding to the simulation of a vehicle in which only a term of the regulator is disabled, the yaw controller. In this way, it is possible to evaluate the contribution of different part and subsystem of the regulator. It is interesting to notice that a good directional stability is also assured when the yaw controller is disabled: as previously introduced in Section 4.2, an optimal allocation of longitudinal traction efforts respect to available adhesion levels is able improve directional stability of the vehicle since higher lateral efforts should be exchanged if the friction ellipse is not completely saturated by high longitudinal tangential forces. On the other hand, it is possible to demonstrate that when the simulated scenario involves heavy yaw torque disturbances, it is the yaw controller to play a key role in assuring vehicle stability.

In Figures 22 and 23, it is proposed the example of a simulation scenario in which adhesion on left wheels is much more degraded with respect to right ones: this condition is simulated both in traction (Figure 22) and braking (Figure 23) conditions imposing value of μ of 0.2 on left tyres and of 0.5 on right ones.

Figure 17 Comparison of the trajectories of the vehicle during a braking from a starting speed of 90 km/h with a wheel road friction coefficient of 0.2. On the left the corresponding graphical representation including 3D contact force measurements on tyres (see online version for colours)

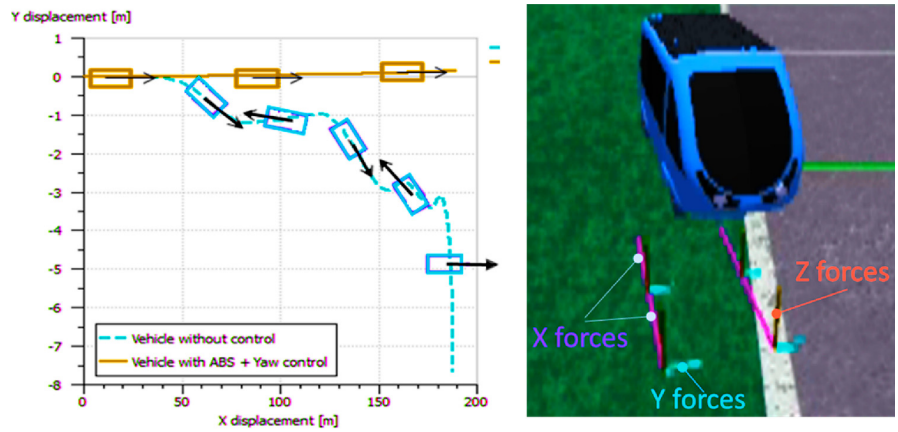

Figure 18 Braking with degraded adhesion, modulated torque on frontal-right wheel (see online version for colours)

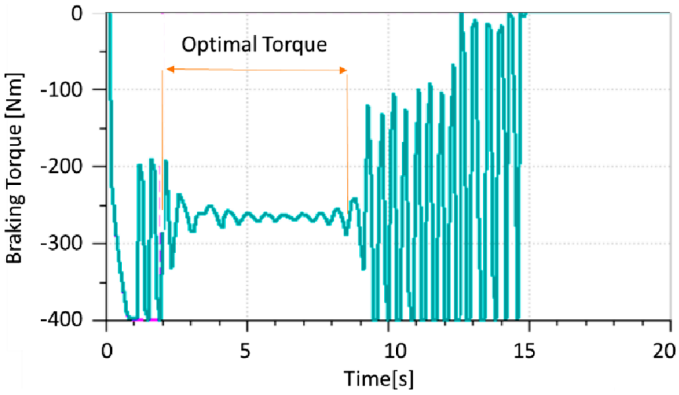

Figure 19 Braking with degraded adhesion, comparison of wheel speed for controlled and uncontrolled system (forward right wheel) (see online version for colours)

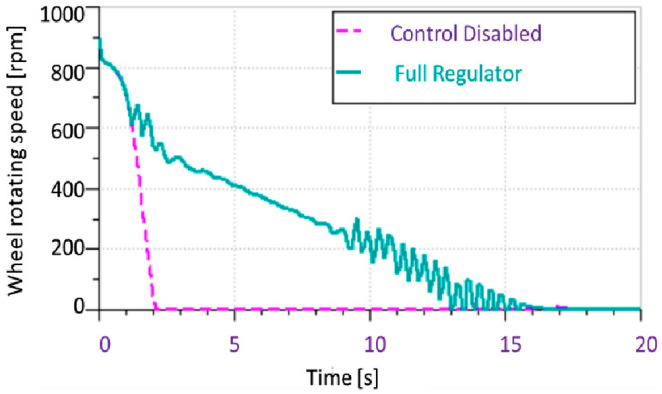

Figure 20 Comparison of the trajectories of the vehicle during traction from 0 km/h to 90 km/h (see online version for colours)

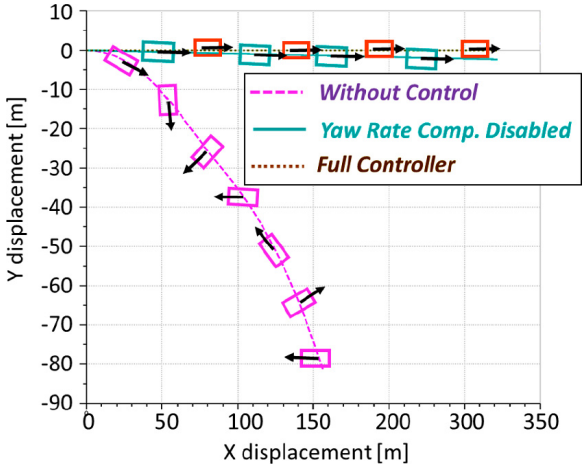

Figure 21 Comparison of the trajectories of the vehicle during traction from 0 km/h to 90 km/h (enlarged detail) (see online version for colours)

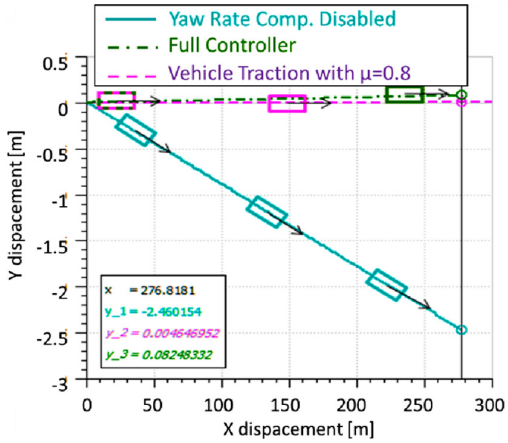

Figure 22 Comparison of the trajectories of the vehicle during traction from 0 km/h to 90 km/h with different adhesion levels between left (μ = 0.2) and right wheels (μ = 0.5) (see online version for colours)

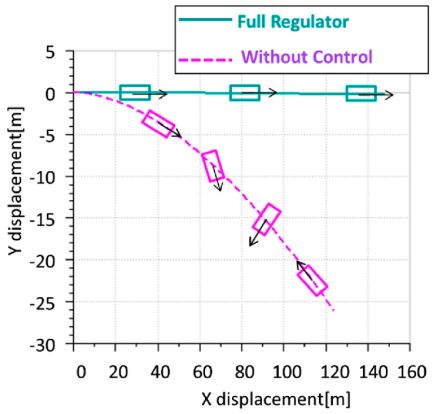

Figure 23 Comparison of the trajectories of the vehicle during braking from 90 km/h to 0 km/h with different adhesion levels between left (μ = 0.2) and right wheels (μ = 0.5) (see online version for colours)

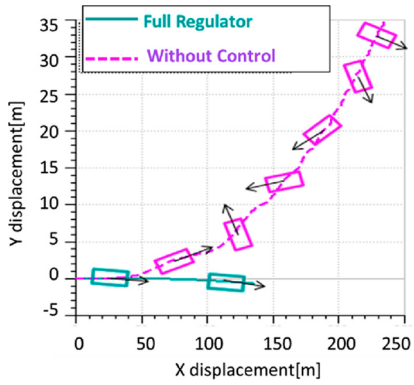

As shown in both figures the regulator, thanks to the contribution of the yaw rate controller, is able to keep stable the trajectory of the vehicle which becomes clearly unstable if the regulator is turned off.

It is also interesting to notice that both braking and traction performances in both cases are better than expected especially for braking simulations: since the minimum adhesion level available on wheels is about 0.2, the authors expected a braking distance of about 150–180 [m]. In the case corresponding to results of Figure 23, the braking distance is 145.8 [m] so it is a bit shorter with respect to the minimum expected. This event can be clearly explained considering both some of the features of the proposed system and the properties of the friction ellipse:

- Vehicle speed estimation algorithm: in the proposed regulator vehicle speed estimation is performed from wheel speed measurements. With two wheels (the right ones) almost in full adhesion conditions estimated vehicle speed and state of wheels are calculated almost exactly maximising the performances of the algorithm.
- During braking, the yaw controller is able to keep stable the vehicle trajectory with a small drift which is also imposed to right wheels which are almost in full adhesion conditions. The phenomenon introduces some light additional losses that contribute to dissipate a bit more energy than expected.

Generally, in more realistic scenarios like mixed adhesion pattern in which the adhesion levels on wheel are different or time variant, the proposed algorithm exhibits higher performances making author quite confident of high robustness of the system in real operating conditions.

7 Conclusions and future developments

In this case, the study authors have proposed the design of an electric van with four in-wheel drive motors. First the study has demonstrated the feasibility of the proposed solutions using standard automation components and technologies implementing an innovative cross transfer of technologies that are mature in robotic and automation fields but rather innovative for the automotive one. A four in-wheel solution is naturally superior than a conventional one in terms of energy efficiency especially in terms of recovered power during a regenerative braking manoeuvre. The main consequences are an increase of the vehicle range in urban traffic conditions and a reduction of the wear of conventional friction brake components (pads and discs). Performed simulations demonstrate that higher costs associated to the proposed solutions in terms of motors and drive systems are largely balanced by the easier implementation of different functionality affecting vehicle safety and stability especially with degraded adhesion conditions. On conventional solutions, most of these functionalities are implemented on dedicated subsystems resulting in a quite complex management that should be drastically simplified in the proposed solution. All these advantages are very important especially for vehicles with small medium production series and high level of customisation where cost-performance optimisations of conventional automotive components and sub-systems are less effective with respect to the case of large, highly standardised mass productions.

Acknowledgements

Authors wish to thank all the people of Argos Engineering SRL (Pistoia, Italy), developer of the GSV vehicle that have enthusiastically supported the unfinanced efforts of a small team of researchers.

References

Allotta, B. and Pugi, L. (2013) *Meccatronica: Elementi di Trazione Elettrica, Società Editrice Esculapio*, Bologna, Italy, ISBN: 9788874885855, DOI: 10.15651/978-88-748-8585-5.

Feiqiang, L., Jun, W. and Zhaodu, L. (2009) 'Fuzzy-logic-based controller design for four-wheel-drive electric vehicle yaw stability enhancement', *2009. FSKD'09. Sixth International Conference on Fuzzy Systems and Knowledge Discovery*, IEEE, 14–16 August, 2009, Tianjin, China, Vol. 4, pp.116–120.

Geamanu, M.S., Cela, A., LeSolliec, G., Mounier, H. and Niculescu, S.I. (2011) 'Road condition estimation and longitudinal control for electric vehicles', *2011 11th International Conference on Control, Automation and Systems (ICCAS)*, IEEE, 26–29 October, 2011, KINTEX Gyeonggi-do, Korea (South), pp.599–604.

Hori, Y. (2004) 'Future vehicle driven by electricity and control – research on four-wheel-motored "UOT Electric March II"', *IEEE Transactions on Industrial Electronics*, Vol. 51, No. 5, pp.954–962.

Ifedi, C.J., Mecrow, B.C., Widmer, J.D., Atkinson, G.J., Brockway, S.T.M. and Kostic-Perovic, D. (2012) 'A high torque density, direct drive in-wheel motor for electric vehicles', *6th IET International Conference on Power Electronics, Machines and Drives (PEMD 2012)*, IET, 27–29 March, 2012, University of Bristol, UK, pp.1–6.

Jain, M. and Williamson, S. (2009) 'Suitability analysis of in-wheel motor direct drives for electric and hybrid electric vehicles', *Electrical Power & Energy Conference (EPEC), 2009 IEEE*, IEEE. 22–23 October, 2009, Montreal, QC, Canada, pp.1–5.

Jazar, R.N. (2008) *Vehicle Dynamics, Theory and Application*, Springer, ISBN: 978-0-387-74243-4.

Ko, S., Ko, J., Lee, S., Cheon, J. and Kim, H. (2014) 'A study on the road friction coefficient estimation and motor torque control for an in-wheel electric vehicle', *Proceedings of the Institution of Mechanical Engineers, Part D: Journal of Automobile Engineering*, 0954407014547750.

Larminie, J. and Lowry, J. (2012) *Electric Vehicle Technology Explained*, 2nd ed., Wiley, August, Oxford, UK, ISBN: 978-1-119-94273-3.

M'Sirdi, N., Rabhi, A. and Naamane, A. (2007) 'Vehicle models and estimation of contact forces and tire road frictions', *ICINCO-RA*, 9–17 May, 2007, Angers, France, pp.351–358.

Meli, E., Pugi, L. and Ridolfi, A. (2014) 'An innovative degraded adhesion model for multibody applications in the railway field', *Multibody System Dynamics*, Vol. 32, No. 2, pp.133–157.

Pacejka, H.B. and Bakker, E. (1992) 'The magic formula tyre model', *Vehicle System Dynamics*, Vol. 21, No. S1, pp.1–18.

Pugi, L., Malvezzi, M., Tarasconi, A., Palazzolo, A., Cocci, G. and Violani, M. (2006) 'HIL simulation of WSP systems on MI-6 test rig', *Vehicle System Dynamics*, Vol. 44, Suppl. 1, pp.843–852.

Schaltz, E. (2011) 'Electrical vehicle design and modeling', ın Soylu, S. (Ed.): *Electric Vehicles – Modelling and Simulations*, 1st ed., Chapter 1, INTECH, Croatia, pp.1–24.

Tanelli, M., Savaresi, S.M. and Cantoni, C. (2006) 'Longitudinal vehicle speed estimation for traction and braking control systems', *2006 IEEE Conference on Computer Aided Control System Design, 2006 IEEE International Conference on Control Applications, 2006 IEEE International Symposium on Intelligent Control*, IEEE, 4–6 October, 2006, Munich, Germany, pp.2790–2795.

Wang, J.N., Wang, Q.N., Jin, L.Q. and Song, C.X. (2011c) 'Independent wheel torque control of 4WD electric vehicle for differential drive assisted steering', *Mechatronics*, Vol. 21, No. 1, pp.63–76.

Wang, Q., Yang, Y. and Jin, L. (2011a) 'Research on ABS regulation of electric vehicle driven by in-wheel motors by AMESim co-simulation with Matlab/Simulink', *2011 International Conference on System Science, Engineering Design and Manufacturing Informatization (ICSEM)*, IEEE, 22–23 October, 2011, Guizhou University, Guiyang, China, Vol. 2, pp.227–232.

Wang, Q., Yang, Y., Jin, L. and Wang, J. (2013b) 'Simulation and analysis on ABS performance of electric vehicle independently driven by four wheel motors', *Journal of Convergence Information Technology*, South Korea, Vol. 8, No. 2, pp.133–143.

Wang, Q., Zhai, L., Wang, J. and Feng, H. (2013a) 'Study on acceleration slip regulation torque distribution control strategy for four in-wheel-motors electric vehicle steering', *2013 25th Chinese Control and Decision Conference (CCDC)*, IEEE, 25–27 May, 2013 Guiyang, China, pp.3832–3837.

Wang, R., Chen, Y., Feng, D., Huang, X. and Wang, J. (2011b) 'Development and performance characterization of an electric ground vehicle with independently actuated in-wheel motors', *Journal of Power Sources*, Vol. 196, No. 8, pp.3962–3971.

Watts, A., Vallance, A., Whitehead, A., Hilton, C. and Fraser, A. (2010) 'The technology and economics of in-wheel motors', *SAE International Journal of Passenger Cars-Electronic and Electrical Systems*, Vol. 3, (2010-01-2307), pp.37–55.

Yin, G., Wang, S. and Jin, X. (2013) 'Optimal slip ratio based fuzzy control of acceleration slip regulation for four-wheel independent driving electric vehicles', *Mathematical Problems in Engineering*, Hindawi, London ,UK.

Young, K., Wang, C., Wang, L.Y. and Strunz, K. (2013) 'Electric vehicle battery technologies', *Electric Vehicle Integration into Modern Power Networks*, Springer, New York, pp.15–56.

Appendix 1

Notation

a: Longitudinal distance (x direction) between front axle and vehicle centre of mass, see the scheme of Figure 7 for more details.

α: Slope of the road adopted in the mono-dimensional model of equation (1).

b: Longitudinal distance (y direction) between rear axle and vehicle centre of mass, see the scheme of Figure 7 for more details.

β: Angle defined according to equation (9).

δ: A steering angle defined according equation (4) and used for the simplified planar vehicle model corresponding to equation (5).

δ_L, δ_R: Steering angles of left (subscript 'L') and right (subscript 'R') wheel.

d: Track of the vehicle, transversal distance (y direction) between left and right wheels, see the scheme of Figure 7 for more details.

ΔT_{ASR}: Vector of the four torque corrections applied to the reference T_{ref} in order to keep near to optimal value of the estimated longitudinal slip $\hat{\lambda}_{xij}$ of each wheel. This symbol is first introduced in the scheme of Figure 12.

ΔT_{ASRij}: It is the corresponding scalar component of the correction vector ΔT_{ASR} applied on the ij wheel.

ΔT_{relij}: It is the corresponding scalar component of the correction applied on the ij wheel ΔT_{ASRij} scaled respect the common torque reference T_{ref}.

ΔT_{YAW}: Vector of the torque corrections applied to the torque references T_{ref*} in order to further correct the directional stability of the vehicle. This symbol is first introduced in the scheme of Figure 12. ΔT_{YAWij} is the corresponding scalar component of the correction applied on the ij wheel.

ΔT_{YAWij}: It is the corresponding scalar component of the correction vector ΔT_{YAW} applied on the ij wheel.

ΔT_{rel_ψ}: As defined in equation (14), it is a relative scaling factor of the yaw correction that is used for a fast calculation of ΔT_{YAWij}.

F: Longitudinal traction force applied to a vehicle (mono-dimensional model along the longitudinal direction), first used in equation (1).

F_d: Longitudinal force due to aerodynamic resistances/drags, first used in equation (1).

F_l: Vertical force due to aerodynamic lift forces, first used in equation (1).

F_{rot}: Longitudinal force corresponding to rolling friction resistances, first used in equation (1).

F_x, F_z: Longitudinal and vertical forces in the quarter vehicle model of Figure 6.

F_{ijk}: Forces exchanged between wheel and road in the simplified planar model of Figure 7; subscript i represents the orientation of the force respect to a reference system which have the longitudinal direction 'x' and transversal one 'y' aligned respectively to peripheral tyre speed and wheel rotation axis; subscript 'j' is used to describe if the wheel is a part of front ('F') or rear ('R') axle; subscript 'k' is referred identify wheel on left ('L') or right ('R') side of the vehicle.

F_{ijkmax}: Maximum force that can be exchanged between wheel and road, see the definition of F_{ijk} for more details on i, j, k subscripts. This symbol is first adopted in relation (7).

$F_{ijkmax*}$: Maximum force that can be exchanged between wheel and road respect to an assigned value of the transmitted force in the perpendicular direction; see the definition of F_{ijk} for more details on i, j, k subscripts. This symbol is introduced in the scheme of Figure 9.

g: Gravitational acceleration (approx. equal to 9.81 ms^{-2}), first used in equation (1).

J: Equivalent rotational inertia of the wheel according the quarter vehicle model of Figure 6.

λ: Relative sliding/slip defined according equation (3).

λ_{ij}: Relative sliding of the *i-j* wheel where *i* indicates front (*F*) or rear (*R*) axle and *j* is used to recognise the right (*R*) or left position of the wheel (*L*) respect to vehicle advance direction.

λ_{kij}: *k* scalar component of the relative sliding/slip of the *i-j* wheels (se also λ_{ij}) respect to the *k* axis. In particular *k* index can have two values '*x*' (longitudinal direction respect to wheel *ij*) and '*y*' (transversal direction respect to the wheel *ij*).

$\hat{\lambda}_{kij}$: Estimated value of the relative sliding component λ_{kij}.

λ_{opt}: Optimal value of the relative slip, able to maximise the adhesion coefficient (see Figure 8 for more details).

m: Vehicle mass, first used in equation (1).

m_t: Equivalent longitudinal vehicle mass considering also the contribution of rotating masses (wheels, motors, etc); first used in equation (1).

μ: Wheel-road friction factor adopted in the quarter vehicle model of Figure 6.

μ_x, μ_y: Wheel-road friction factor along longitudinal (*x*) and transversal (*y* direction) respect to the wheel as first used in equation (8).

r: Rolling radius of the wheel.

ρ: Density of air, first used in equation (1).

S: Equivalent frontal section of the vehicle for the calculation of aerodynamic forces; this symbol is first used in equation (1).

T_m: Torque applied on the wheel according the quarter vehicle model of Figure 6.

T_{ref}: Common reference torque to be applied to each motorise wheel according the performed manoeuvre of the human driver as described in Figure 12.

T_{ref*}: As described in the scheme of Figure 12, it is the vector of torque reference values that have been generated after the application of the correction ΔT_{ASR}. T_{ref*ij} is used to identify the *ij* element of the T_{ref} vector.

T_{ref**}: It is the vector of torque reference values that have been generated after the application of the correction ΔT_{YAW} to torque references T_{ref*}. This symbol has been first introduced in the scheme of Figure 12.

$x, \dot{x}, \ddot{x}$: Longitudinal position and its time derivatives, (speed and acceleration). these symbols are first introduced in equation (1).

$x_*, \dot{x}_*, \ddot{x}_*$: Estimated vehicle position and its time derivatives considering also the slew-rate limitations implemented in equation (10).

$x_*, \dot{x}_*, \ddot{x}_*$: Estimated position and its time derivatives as estimated from wheel tachometers according (10).

$x_{imu}, \dot{x}_{imu}, \ddot{x}_{imu}$: Position and its time derivatives as estimated by IMU sensors (inertial measurement units produce a direct estimation of accelerations and derived ones of speed and displacement from numerical integration and data fusion of inertial measurements).

x_{ideal}: It is the value of the braking distance supposing optimal/ideal condition in terms of distribution of braking forces between wheels, it is an optimal asymptotic value defined according equation (16).

x_{stop}: Simulated braking distance considering real vehicle performances and adhesion conditions.

$\dot{x}_{init}$: Initial speed considered for the calculation of both ideal and real braking distances.

$\psi, \dot{\psi}, \ddot{\psi}$: Angular yaw of vehicle carbody and its derivatives.

$\hat{\dot{\psi}}$: Estimated/measured value of the yaw rate of vehicle carbody.

$\hat{\dot{\psi}}_{opt}$: Optimal value of the yaw rate considering optimal steering conditions as defined in equation (13).

v_{ch}: Transversal drift effect introduced in equation (13) to roughly tune the simplified steering model respect to real performances of the simulated tyre.

ω: Rotational speed of the wheel in the quarter vehicle model of Figure 6.

Abbreviations

ABS: Anti-lock braking system

ASR: Anti slip regulation, a system able to limit excessive slip during traction, often used as synonymous of TCS

EV: Electric vehicle

ECE UDC: European Community Urban Driving Cycle often also the shortest acronyms ECE or UDC are used to describe the same cycle

GSV: Green shuttle vehicle, the commercial name of the prototype object of this study

ICE: Internal combustion engine

MIMO: Multiple input multiple output system

NEDC: New European driving cycle, is a more recent version European cycle for testing of ground vehicles is substantially composed by the repetition of four ECE-15 urban drive cycles followed by sequence of manoeuvres at various speed between 80 km/h and 120 km/h.

PM: Permanent magnet motor

TCS: Traction control system